Atmos. Chem. Phys. Discuss., https://doi.org/10.5194/acp-2017-946
Manuscript under review for journal Atmos. Chem. Phys.
Discussion started: 13 October 2017

Atmospheric Chemistry and Physics
Discussions

Statistical Analysis of Contrail to Cirrus Evolution during the Contrail and Cirrus Experiments (CONCERT)

Aurélien Chauvigné[1], Olivier Jourdan[1], Alfons Schwarzenboeck[1], Christophe Gourbeyre[1], Christiane Voigt[2,3], Hans Schlager[2], Stefan Kaufmann[2], Stephan Borrmann[3,4], Sergej Molleker[3,4], Andreas Minikin[2,5], Tina Jurkat[2], Ulrich Schumann[2]

[1]Laboratoire de Météorologie Physique, UMR 6016 CNRS/Université Clermont Auvergne, Clermont-Ferrand, France.
[2]Institut für Physik der Atmosphäre, Deutsches Zentrum für Luft- und Raumfahrt (DLR), Oberpfaffenhofen, Germany.
[3]Institut für Physik der Atmosphäre, Universität Mainz, Mainz, Germany.
[4]Max-Planck-Institute for Chemistry, Department for Particle Chemistry, Mainz, Germany.
[5]Now at: Flugexperimente, Deutsches Zentrum für Luft- und Raumfahrt (DLR), Oberpfaffenhofen, Germany.

Abstract:

Air traffic affects the cloudiness, and thus the climate, by emitting exhaust gases and particles. The study of the evolution of contrail properties is very challenging due to the complex interplay of vortex dynamics and atmospheric environment (e.g. temperature, supersaturation). Despite substantial progress in recent years, the optical, microphysical, and macrophysical properties of contrails and ambient cirrus during contrail formation and subsequent ageing are still subject to large uncertainties due to instrumental and observational limitations and the large number of variables influencing the contrail life cycle. In this study, various contrail cases corresponding to different aircraft types and atmospheric conditions are investigated using a statistical method based on the in situ optical measurements performed during the CONCERT campaigns 2008 and 2011. These two aircraft campaigns encompass more than 17 aircraft contrail cases. A Principal Component Analysis (PCA) of the angular scattering coefficients measured by the Polar Nephelometer has been implemented in order to classify the sampled ice cloud measurements in 6 clusters representative of different development stages of the contrails (primary wake, young contrail, contrail-cirrus and natural cirrus). Based on the information derived from air traffic control, extinction coefficients, asymmetry coefficients, nitrogen oxide concentrations, relative humidity with respect to ice (RHI) and particle size distributions are analyzed for each cluster to provide a characterization of the evolution of ice-cloud properties during the contrail to cirrus evolution. The PCA demonstrates that contrail optical properties are well suited to identify and discriminate the different contrail growth stages and to provide an independent method for the characterization of the evolution of contrail properties.

1 Introduction

Aircraft exhaust plumes have a significant impact on climate and tropospheric chemistry (Lee et al., 2010; IPCC, 1999). The Intergovernmental Panel for Climate Change IPCC special report on aviation (1999) estimates that NO_x emissions from subsonic aircraft increase ozone concentrations by up to 6% at cruise level. Short and long lived pollution species have different impact on atmospheric chemical composition depending on the flight level (Frömming et al, 2012). Emissions of water vapor, black carbon (BC) / soot particles, sulfate (SO_4) aerosols and nitrogen oxides (NO_x) contribute to the modification of the chemical composition of the upper troposphere on shorter timescales (Lee et al., 2010, Gettelman and Chen, 2013; Liou et al., 2013). The long term climate impact is mainly driven by CO_2 emissions. Modelling studies have shown that the direct radiative forcing from aviation is expected to represent 3-4% (50-60 mW m^{-2}) of the anthropogenic forcing (Lee et al., 2010; De Leon et al., 2012) and could reach 87 mW m^{-2} in 2025 (Chen and Gettelman, 2016). Aircraft induced cloudiness has also an important impact on climate, although the quantitative assessment of the radiative forcing remains a major source of uncertainties (Lee et al., 2010).

Contrail formation is mainly controlled by the thermodynamic properties of the ambient air and by the aircraft emissions. The conditions for contrail formation can be determined by the Schmidt-Appleman Criterion (SAC) (Schumann, 1996). Contrail chemical composition can have a significant impact on the contrail formation (Kärcher et al., 2009). Indeed, the emission index (e.g. soot emission index in kg-fuel^{-1}) is directly linked to the contrail microphysical properties, as the total number densities and ice crystal diameters. Several studies in the past have been dedicated to the evolution of concentrations of nitrogen oxide (NO) and sulfur dioxide (SO_2). Rapidly oxidized by OH (post-combustor reaction; Jurkat et al., 2011), NO and SO_2 are transformed into a series of species including nitrous acid (HONO), nitric acid (HNO_3), and sulfuric acid (H_2SO_4). Part of the nitric acid, e.g., formed in the young plume is taken up by contrail ice particles (Kärcher and Voigt, 2006; Voigt et al., 2006; Schäuble et al., 2009). HONO can be a temporary reservoir of OH by photolysis reactions, and H_2SO_4 a precursor for radiatively active sulfate particles also contributing to soot particle coating (Jurkat et al., 2011). OH-induced reactions, formation and reaction schemes of greenhouse gases (H_2O, O_3, CH_4), as well as emission of black carbon and sulfate aerosols have significant impact on climate (Frömming et al., 2012; Gettelmann and Chen, 2013). Two different processes of contrail formation have been studied: combustion condensation trails and aerodynamic condensation trails. Different studies (Gierens and Dilger, 2013; Jansen and Heymsfield, 2015) have illustrated characteristics of aerodynamically controlled contrail formation associated to warmer temperatures (observations at temperatures above -38°C). For contrails primarily initiated by the combustion processes, the mixing of hot and humid exhaust gases with cooler and dryer ambient air increases the local relative humidity in the exhaust plume leading to the formation of contrails when the saturation with respect to liquid water is reached. Thus, soot and sulfate aerosols emitted by the aircraft (Moore et al., 2017) may act as condensation nuclei to form liquid droplets. Homogeneous ice nucleation of the liquid droplets can occur when the exhaust cools down through mixing with the ambient temperature, while preserving ice saturation. Small ice crystals are then formed in the jet phase within some tenths of a second (Kaercher and Yu, 2009). The further life-cycle of contrails depends on the interaction with the wake vortices behind aircraft and the ambient atmosphere (Irvine et al., 2012; Graf et al., 2012; Duda et al., 2013; Carleton et al., 2013; Schumann and Heymsfield, 2017). The ice crystals in the young contrails are captured within two counter-rotating wake vortices in the downwash behind the aircraft induced by the aircraft lift, which induce adiabatic compression, heating, and partial sublimation of the ice crystals within the primary wake (Lewellen and Lewellen, 2001; Sussmann and Gierens, 2001, Unterstrasser et al., 2008, Unterstrasser et al., 2016; Kärcher and Voigt, 2017). This primary wake may disappear if ambient air is subsaturated with respect to ice. In the case of supersaturation, the secondary wake becomes visible, thereby detraining ice particles from the primary wake at a higher level (Sussmann and Gierens, 1999, Kaufmann et al., 2014). The initially almost spherical ice crystals become increasingly aspherical and grow by uptake of water vapor as long as saturation with respect to ice is prevailing. For ambient humidity above ice saturation, contrails can persist after the vortex breakdown, spread and evolve into contrail cirrus (Schumann and Heymsfield, 2017). The associated cloud cover (larger than for linear contrails alone) of contrail cirrus then shows increasing impact on the radiative forcing (Burkhardt and Kärcher, 2011; Schumann et al., 2015).

The assessment of the contrail radiative forcing requires, in particular, an accurate estimation of the cloud cover, the visible optical depth, the single scattering characteristics, the ice crystal effective size and habit (Yang et al., 2010; Spangenberg et al., 2013). Satellite observations provide a comprehensive dataset to study statistically the contrail to cirrus evolution. The combined contrail tracking algorithms on the Spinning Enhanced Visible and Infrared Imager (SEVIRI) on board the Meteosat Second Generation (MSG) satellites with properties inferred by the Moderate Imaging Spectroradiometer (MODIS) on board the Terra satellite was used by Vazquez-Navarro et al., (2015) to characterize the properties of 2300 contrails. Properties included lifetime (mean values of 1h), the width (8 km), the length (130 km), the optical thickness (0.34), the altitude (11.7 km) and the radiative forcing (-26 W m^{-2} for shortwave forcing over land) of these contrails. However, detailed in situ optical and microphysical measurements are still needed to evaluate satellite products and to develop more appropriate retrieval algorithm. In particular, distinguishing contrails from natural cirrus remains extremely challenging from satellite observations. Although the optical and microphysical properties of young contrails (linear contrails) differ from natural cirrus properties, the contrail properties are highly time dependent and persistent contrail cirrus can be embedded in thin cirrus clouds. Recent *in situ* measurements (Voigt et al., 2017) show that the microphysical properties of contrail cirrus can still be distinguished from natural cirrus at contrail cirrus ages up to several hours.

Most of the studies (Jessberger et al., 2013; Lewellen et al., 2012; Schumann et al., 2013) separate the contrail analysis between the two wakes. Indeed, the primary and secondary wake properties depend strongly on atmospheric conditions and aircraft type (emission index, vortex, flight level, ambient humidity, temperature,…). In the primary wake, contrail ice crystals are quasi-spherical with values of the effective diameter (Deff) typically lower than 4 µm (Schumann et al., 2011; Gayet et al., 2012; Järvinen et al., 2016; Schumann et al., 2017b). Also the total number concentration of ice particles is typically larger than 1000 cm^{-3} a few seconds after contrail formation (Baumgardner and Gandrud, 1998; Petzold et al., 1997) and subsequently decreases by dilution to concentrations below 200 cm^{-3} within less than a minute after contrail generation (Poellot et al., 1999; Schröder et al., 2000; Gayet et al., 2012). Gayet et al. (2012) reported mean values of ice water content of 3 mg m^{-3} and maximum extinction coefficients close to 7 km^{-1}. The recent overview on contrail studies presented in Schumann et al. (2017b) reports several microphysical properties at different stages, for different atmospheric conditions as well as comparisons with the Contrail Cirrus Prediction (CoCIP) model simulations. Their study highlights a large variability (which increases with contrail age) of contrail properties. Comparing primary and secondary wakes, several studies reported findings on the secondary wake and its evolution into contrail cirrus. Detrained from the primary wake and submitted to saturated ambient air with respect to ice, ice crystals grow rapidly, while crystal concentration decreases. Within the first minutes after formation, measurements exhibit aspherical ice crystals characterized by effective sizes up to 6 µm, IWC ranging between 2.5 and 10 mg m^{-3}, extinction between 2 and 3 km^{-1}, with crystal concentrations typically lower than 100 cm^{-3} (Goodman et al., 1998; Voigt et al., 2010; Kübbeler et al., 2011; Gayet et al., 2012; Jeßberger et al., 2013; Schumann et al., 2013; Poellot et al., 1999; Febvre et al., 2009; Kaufmann et al., 2014). Aged contrails can persist and evolve into contrail cirrus if the ambient air is saturated with respect to ice, however those studies are limited by the lack of unambiguous identification (Schumann et al., 2017a). Also after a few minutes, difficulties appear for the pilot to track the contrail by visual navigation, which is due to contrail and contrail cirrus spreading in the free troposphere. Observations of the ice crystal shape and growth over several tens of minutes and up to an hour illustrate that crystal effective size can easily reach 20 µm and beyond with number concentrations ranging from 1 to 5 cm^{-3} (Lawson et al., 1998; Schäuble et al., 2009), extinction less than 0.5 km^{-1} (Febvre et al., 2009), and IWC up to 10 mg m^{-3} (Schröder et al., 2000; De Leon et al., 2012). At this stage, within a sustained ice-supersaturated environment, contrail microphysical properties may still differ from those of natural cirrus (Voigt et al., 2017) with concentrations of ice crystals larger than 100 µm in the order of 0.1

Atmos. Chem. Phys. Discuss., https://doi.org/10.5194/acp-2017-946
Manuscript under review for journal Atmos. Chem. Phys.
Discussion started: 13 October 2017

Atmospheric Chemistry and Physics
Discussions

cm^{-3}. These crystals typically show bullet rosette type habits (Heymsfield et al., 1998; Heymsfield et al., 2010). Optical depth values can reach a value of 2.3 (Atlas and Wang, 2010), corresponding to an extinction of 0.023 km^{-1}. Nevertheless, the transition from contrails to cirrus highly depends on the ambient saturation conditions and modelling studies with typical atmospheric conditions suggest time evolution of optical and microphysical properties from contrail to contrail cirrus clouds (Burkhardt and Kärcher, 2011; Unterstrasser et al., 2016 ; Schumann et al., 2015).

In this study, we report on a method presenting a powerful alternative for classifying cloud events into young contrail, contrail-cirrus and natural cirrus. The method is applied to aircraft data of the CONCERT (Contrail and Cirrus Experiment) campaigns (Voigt et al., 2010, 2011, 2014). The methodology consists of implementing a principal component analysis (PCA) of the angular light scattering data from a Polar Nephelometer. The PCA results of the different type of contrails (different clusters) are then utilized with corresponding optical, microphysical, and chemical properties in order to validate hypothesis on contrail phase definitions (young contrails to cirrus contrails). This paper starts with an illustration of the properties of contrails and cirrus clouds observed during two specific CONCERT flights (19 November 2008 and 16 September 2011) encompassing a series of different contrail evolution phases. These two flights containing a variety of contrail-cirrus information can be regarded as an analytical framework producing results which then can be compared to contrail-cirrus properties of other flights.

2 CONCERT projects and data processing

2.1 CONCERT campaigns

CONCERT-1 and CONCERT-2 campaigns took place in October/November 2008 and August/September 2011, respectively. These two campaigns with the DLR Falcon 20 E research aircraft were based in Oberpfaffenhofen, Germany, and sampled contrails and cirrus at mid-latitudes in the Northern Hemisphere. The overall objective has been to reduce uncertainties on the microphysical, chemical, and radiative properties of contrails behind aircraft of different types and to improve the evaluation of contrail's impact on climate. Besides the primary objectives focusing on contrails, few CONCERT flights were dedicated to emissions of Etna and Stromboli volcanos (Voigt et al., 2014; Shcherbakov et al., 2016). Also a few stratospheric intrusions were observed during the flight missions. In total, 23 flights were recorded during the two measurement campaigns, wherein 12 flights were entirely focused on aircraft contrail chasing. Overall, more than 17 different aircraft exhausts plumes have been probed. Particularly, the CONCERT-2 campaign mainly focused on observing persistent contrails, and hence on the evolution of contrails into contrail cirrus.

During both CONCERT campaigns, the DLR research aircraft Falcon was equipped with a set of instruments to measure the optical and microphysical properties of cloud particles and also the trace gas composition in the UTLS (Upper Troposphere / Lower Stratosphere) region. Voigt et al. (2010) provide a detailed description of the aircraft instrumentation. We briefly introduce the instruments used in this study.

2.2 Aircraft instrumentation

The microphysical and optical particle properties of contrails and cirrus presented in this study were mainly derived from the PMS Forward Scattering Spectrometer Probe 300 (FSSP-300), the Polar Nephelometer (PN), and the PMS 2D-C hydrometeor imaging probe. The combination of these independent techniques characterizes cloud particles within a range of diameters varying from 0.5 µm to 2 mm.

The PN (Gayet et al., 1997) measures the angular scattering coefficients (non-normalized scattering phase function) of an ensemble of water droplets or ice crystals or a mixture of those particles ranging from a few micrometers to approximately 1 mm in diameter. These particles intersect a collimated laser beam, at a wavelength of 804 nm, near the focal point of a parabolic mirror. The light scattered at angles from 3.49° to 172.5° is reflected onto a circular array of 56 near-uniformly positioned photodiodes. In this study, reliable measurements were performed at 30 scattering angles ranging from ±15° to ±162°. The measurements allow to distinguish particle phase (water droplets or ice crystals) and to derive single scattering properties such as the extinction coefficient and the asymmetry coefficient with uncertainties of 25% and 4%, respectively (Gayet et al., 2002; Jourdan et al., 2010).

Particle size distributions and corresponding microphysical and optical integrated properties (IWC, Deff, N, and extinction) were derived from FSSP-300 measurements (Baumgardner et al., 1992). This instrument measures the intensity of forward scattered light from cloud particles passing through the laser beam, with cloud particles in the diameter range 0.35-20 µm. In the forward angular region (from 4° to 12°), scattering is mainly described by the particle diffraction pattern and therefore depends on the refractive index, the shape, and the size of the particles. The method of data processing and size calibration used during the CONCERT campaigns have been presented in Gayet et al. (2012) (Appendix A). We briefly recall that the asymmetry parameter derived from the PN was used to discriminate nearly spherical particles ($g \geq 0.85$) from non-spherical ones ($g < 0.85$) at 804 nm. For spherical ice particles, Mie calculations were used to derive the size bin limits and the corresponding extinction efficiency. Results were adjusted to the calibrated probe response. Additionally, in order to minimize Mie ambiguities related to the FSSP-300 size response, 31 channels were rebinned to 13 channels with a diameter ranging from 0.5 µm to 18 µm (upper channels 30 and 31 were excluded from the data analysis). For non-spherical particles, the size of the contrail particles is expressed in terms of an equivalent surface or area diameter, i.e. the diameter of a sphere that has the same area than the projected area of the measured non spherical particle image (Mishchencko et al., 1997; Schumann et al., 2011). The particles were assumed to be rotationally symmetric ice ellipsoids with an aspect ratio of 0.5. Accordingly, and contrary to the method used for spherical particles, 15 size bins ranging from 0.5 µm to 18 µm were defined based on T-Matrix calculations following Borrmann et al., (2000).

The bi-dimensional optical array spectrometer probe (2DC) provides information on the crystal size and shape within a nominal size range from 25 µm to 800 µm by recording cloud particles shadow images with a 25 µm resolution. The method of data processing used in this study is described in detail in Gayet et al. (1996) and Febvre et al. (2009). Reconstruction of truncated particles has been considered for the PSD calculations and the sampling surfaces have been derived according to Heymsfield and Parrish (1978). In order to improve the statistical significance of low particle concentrations, a 5-s running mean was applied. The bulk parameters were calculated assuming the surface-equivalent diameter relationships of Heymsfield (1972) and Locatelli and Hobbs, (1974). As the sensitivity of the probe to small particles decreases with airspeed (Lawson et al., 2006), particles smaller than 100 µm may not be detectable at the Falcon airspeed of typically 180 m s^{-1}. This may result in larger uncertainties of up to 100% in the derived microphysical parameters such as the IWC (Gayet et al., 2002 and 2004).
Depending on the spherical or non-spherical shape of ice crystals, ice water content IWC, extinction coefficient Ext, and effective diameter D_{eff} were calculated independently according to Garret et al. (2003) and Gayet et al. (2012). For spherical ice crystals ($gPN \geq 0.85$), optical and microphysical properties are calculated from the following equations:

$$Ext = \frac{\pi}{4} \sum_i \beta_{ext}^i N_i D_i^2 \quad (1)$$

$$IWC_{spherical} = \frac{\pi}{6} \rho_{ice} \sum_i N_i \, D_i^3 \quad (2)$$

where β^i_{ext} is the extinction efficiency (depending on spherical or aspherical particle characterization), D_i the mean diameter in channel i, N_i the number concentration, and ρ_{ice} the bulk ice density (0.917 g cm^{-3}).

For non-spherical ice crystals (gPN < 0.85 and for particle diameters larger than 70 µm), an equivalent diameter method is used (Gayet et al., 2004). For an ice crystal with an area A, the particle equivalent diameter D_{equ} and equivalent mass x_{equ} are defined as :

$A \leq 0.049$ mm² $\qquad D_{equ} = 0.82\, A^{0.48}$ (3)

$A > 0.049$ mm² $\qquad D_{equ} = 0.56\, A^{0.32}$ (4)

$$x_{equ} = \frac{\pi}{6} \rho_{water} {D_{equ}}^3 \quad (5)$$

$$IWC_{non-spherical} = \rho_{ice} \sum_i N_i x_{equ} \rho_{water} \quad (6)$$

With ρ_{water} the bulk water density (1 g cm^{-3}).

In young tropospheric aircraft plumes, the main chemical component to be measured is NO_y, mainly composed of NO and NO_2. During CONCERT campaigns trace gas measurements of NO and NO_y mixing ratio were performed using the chemiluminescence technique (Schlager et al., 1997) with a time resolution of 1 s. The accuracy (and precision) of the NO and NO_y measurements are estimated with 7% (and 10%) and 10% (and 15%), respectively (Ziereis et al., 2000).

Chemical ionization mass spectrometry combined with a SF_5^- ion source was used to detect the concentration of HNO_3, SO_2, and HONO in the exhaust plumes and the UTLS (Jurkat et al., 2010, Jurkat et al., 2011). Mass spectra were sampled with an ion trap mass spectrometer with resolution of < 0.3 atomic mass units and averaged over five spectra resulting in an overall time resolution of 1.6 s. Detection limits for HONO and SO_2 for 1.6 s time resolution were 72 and 67 pmol mol^{-1} and for HNO_3 36 pmol mol^{-1} for 32 s time resolution. During CONCERT 2011 a quadrupole mass spectrometer was employed on the Falcon (Voigt et al., 2014) with detection limits of 15 pmol mol^{-1} for HNO_3 and 8 pmol mol^{-1} for SO_2 at 20 s time resolution (Jurkat et al., 2016).

The detection of water vapor and relative humidity with respect to ice (RHI) is important to characterize contrail ice crystals. Water vapor has been measured with the chemical ionization mass spectrometer AIMS-H2O during CONCERT-2 (Kaufmann et al., 2014; 2016). In addition, hygrometers using the Lyman-α technique (Zöger et al., 1999; Meyer et al., 2015), and frost point hygrometers (Heller et al., 2017) were implemented on the Falcon during CONCERT-1 and 2.

3 Results

3.1 Overview of the cloud properties sampled during the reference cases

The purpose of this section is to give an overview of the contrail optical properties and more interestingly to evaluate the ability of the Polar Nephelometer measurements to identify contrails. Two flights, performed on 16 September 2011 during CONCERT-2 (flight 16b) and on 19 November 2008 during CONCERT-1 (flight 19b), respectively, were selected for their variety of contrails and cirrus sampled during these two flights. The two flights are considered as a benchmark to illustrate the potential of the PCA methodology described in Sect. 3.2.

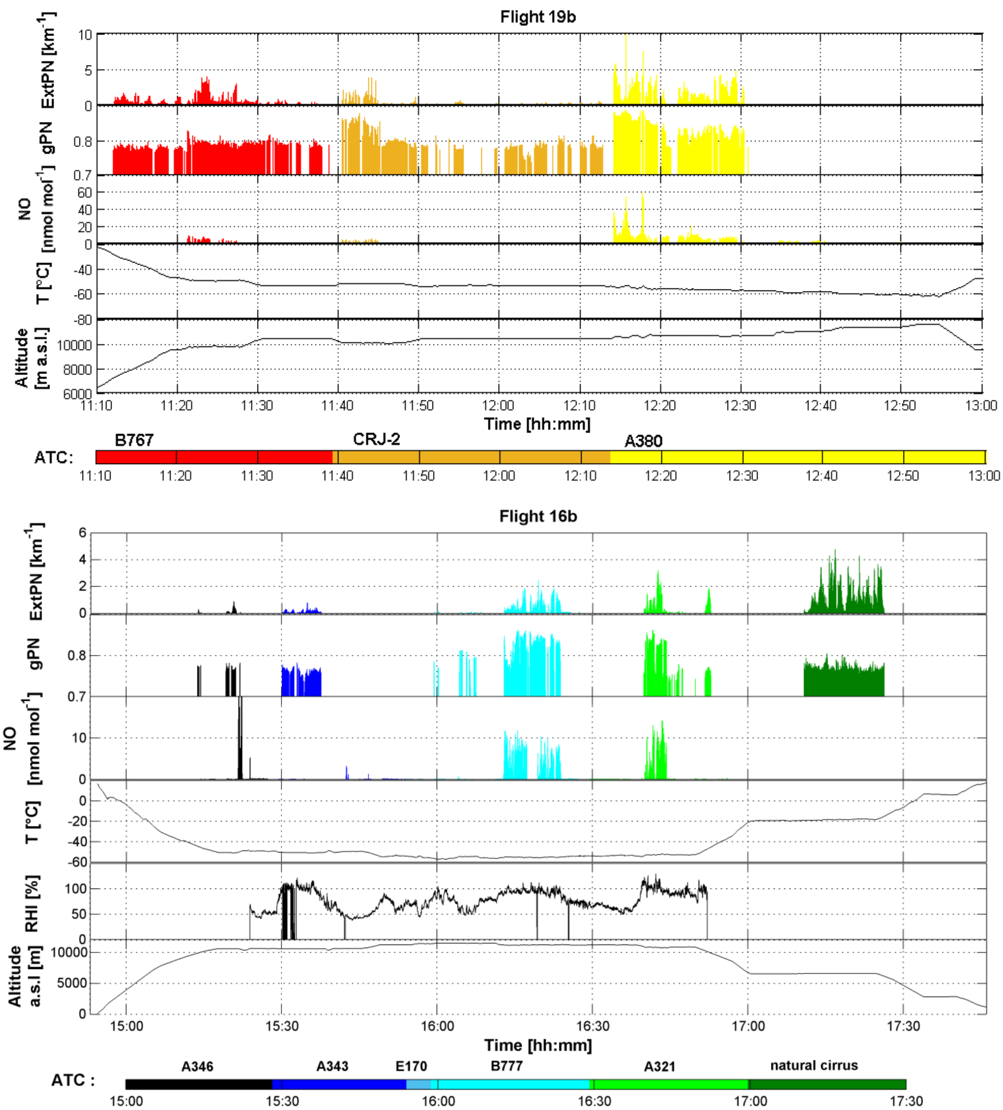

Figure 1 : Time series at 1 s resolution for flights a) 19b and b) 16b. From top to bottom: extinction coefficient (in km^{-1}) and asymmetry parameter measured by the Polar Nephelometer at 804 nm, concentration of nitric oxide (in nmol mol^{-1}) measured by chemiluminescence technique, temperature (in °C), relative humidity with respect to ice (in %), and altitude a.s.l. (in m). Temporal series are colored according to time, and grey indicators illustrate contrail information from Air Traffic Control (ATC) information as provided by a dedicated flight controller.

Figure 1 displays the time series of the extinction coefficient (ExtPN) at 804 nm, asymmetry parameter (gPN) at 804 nm, relative humidity (RHI), and the nitric oxide (NO) concentration for flights 19b and 16b. RHI measured with the AIMS mass spectrometer is shown for flight 16b. For RHI measurements on flight 19b we refer to Kübbeler et al. (2011); Gayet et al. (2012); Jessberger et al. (2013) ; Schumann et al. (2013). For both flights, Air Traffic Control (ATC) provided information on the aircraft characteristics (aircraft type, engine type, fuel flow, weight, engine power setting,…) responsible for the formation of encountered contrails. In a first classification approach, the time series are color coded according to the ATC information of consecutive sampling of different contrails.

The PN Extinction coefficient coupled with the asymmetry parameter seems to be a reasonable proxy to detect contrails and cirrus clouds (see amongst other references, Voigt et al., 2010). ExtPN values, by definition, depend on the cloud particle concentration and size. Values typically beyond 0.1 km^{-1} correspond in general to cloud events well correlated to supersaturation with respect to ice conditions (RHI > 100%). Figure 1 proves that relatively high values of extinction can be found in flights 19b and 16b which are linked to the presence of contrails or cirrus clouds. Moreover, the temporal distributions of these values are coherent with ATC information for both flights. For instance, most of the contrails induced by commercial aircraft exhaust plumes translate into significant extinction coefficient values. The ExtPN values are between 0.2 km^{-1} and 10 km^{-1} for contrails induced by A346, A340, and A380 commercial aircraft. Cirrus clouds are detected with more variable extinction values mostly larger than 0.5 km^{-1}. Most of the aircraft induced contrails are detected by the PN with the exception of the ones stemming from the E170 airplane. At 15:50 during flight 16b, ATC identified the E170 position close to the Falcon flight trajectory, however the ExtPN and the NO mixing ratio remained very low. Hence, the E170 contrail was not probed by Falcon. In the following we assume that only periods with ExtPN values above 0.1 km^{-1} are considered a reasonably reliable signature for contrails sampled during the flight campaigns.

The absolute values of the asymmetry parameter gPN provide additional information of the cloud particle shape. Indeed, gPN is a good indicator of the degree of sphericity of ice crystals (Gayet et al., 2012). Ice clouds with gPN values higher or equal to 0.85 are typically composed of spherical ice crystals, whereas lower values are indicative of aspherical ice particles. In a supersaturated environment of contrails, crystals grow by water vapor deposition and become increasingly aspherical with time. This is why spherical ice crystals prevail in very young contrails with an asymmetry coefficient around 0.85 with RHI above 100%. Subsequently, gPN is decreasing when water vapor diffusion is generating more and more aspherical crystal shapes at ice supersaturation. This can be observed for A321 chasing during flight 16b with gPN decreasing to 0.75 whilst RHI remains around 100%, whereas for B777 chasing, no gPN decrease is observed at RHI < 80%. Also natural cirrus clouds are mainly composed of non-spherical ice crystals, possibly with hexagonal shapes. These clouds can be easily discriminated from young contrails as they exhibit a much lower asymmetry parameter typically below 0.75 (see amongst others Jourdan et al., 2003b, Febvre et al., 2009). However, no accurate ambient RHI data can retrieved for measurements in natural cirrus due to instrumental calibration problems. A good example of the evolution of gPN is the CRJ-2 contrail observed between 11:40 and 11:45 during flight 19b. The sequence illustrates the potential of the gPN measurement to characterize the evolution of contrail properties, with decreasing crystal sphericity documented by the decreasing asymmetry parameter from 0.88 to 0.79 (uncertainties around 0.04) after only 5 min and down to 0.77 after 20 min. A more stable variation of gPN values (around 0.78 ± 0.02) is then observed until 12:10 after 30 min of contrail ageing associated with crystal growth by water vapor diffusion. A similar decrease in gPN has been noted by Gayet et al. (2012) in the ageing contrail from an A380 aircraft and is visible for the B767 and the A321 contrails.

NO concentration measurements can also be used to discriminate natural cirrus clouds from ice clouds influenced by aircraft traffic. At the typical altitude of 10 km, NO environmental concentrations are close to background values. In contrast, NO concentrations in young contrails may reach several tens of nmol mol^{-1} (Voigt et al., 2010). Figure 1 shows a good correlation between the expected localization of young contrails and NO concentrations. The dilution effect into the upper troposphere causes an important decay of chemical concentrations. For instance, the first few seconds of the A380 chasing during flight 19b are characterized by a high NO concentration (up to 40 nmol mol^{-1}) followed by a fast decrease to 10 nmol mol^{-1} in the next 15 min, and less than 5 nmol mol^{-1} beyond 15 min. NO concentrations finally decrease to background levels within hours (e.g. Voigt et al., 2017). This decrease of the NO concentration is in accordance with the decrease of the extinction coefficient (from 10 to 0.2 km^{-1}) and asymmetry parameter (from 0.88 to 0.77). Thus NO was mainly used as additional contrail indicator. However, during some aircraft chasing events, NO concentrations were near background levels, while mass spectrometric measurements (not shown here) indicate elevated concentrations of HONO, HNO_3, and SO_2 representative for contrail chemical species.

The above case studies of flights 19b and 16b clearly show that the optical properties of contrail type ice clouds (supported by the ATC information) in conjunction with specific trace gas concentration measurements can be used to discriminate contrails from natural ice cloud events. A first order analysis of these parameters can be used to roughly distinguish young contrails (mostly quasi-spherical ice crystals) from aged contrails (mostly aspherical ice crystals) and natural cirrus (background NO concentrations). This analysis is mainly qualitative and based solely on a few integrated parameters (Fig. 1). A more robust statistical method should be used to accurately separate the different contrail phases and also natural cirrus. In the following section, relationships between contrail and ice cloud properties and their scattering properties are investigated more extensively to assess whether the information content of the PN scattering measurements is sufficient to document changes in the contrail microphysical properties.

3.2 Statistical Method

In this section, we present a methodology based on the statistical analysis of the optical signature of ice clouds and in particular contrails. The goal is to classify the contrail properties according to the aircraft origin and evolution stage. The main objective of the Principal Component Analysis (PCA) is data reduction in order to allow a better physical interpretation of the light scattering patterns derived from the Polar Nephelometer measurements (Legendre and Legendre, 1998; Jourdan et al., 2003). In this study, optical properties of ice crystals in the evolving contrail environment are analyzed to evaluate contrail evolution. This statistical analysis was already successfully applied to discriminate mixed phase clouds (Jourdan et al., 2010), liquid clouds, and ice clouds, (Jourdan et al., 2003) as well as to characterize porous aerosol in degassing plumes (Shcherbakov et al., 2016) using light-scattering properties measured by the Polar Nephelometer.

3.2.1 Reference definition

The PCA is first applied to the PN angular scattering coefficients measurements performed during flights 16b and 19b which are here considered as our reference datasets. Initially, a correlation matrix is calculated to characterize the link between each scattering angle. The PCA is designed to generate a new limited set of uncorrelated parameters, called principal components C_{lj} representative of the original data set variability.

A first implementation of the PCA is performed to detect unreliable data or out of order photodiodes. For instance, seven photodiodes presented a low signal to noise ratio and were excluded from the dataset. Flight sequences characterized by ExtPN<0.1 were also removed. Finally, flight sequences dedicated to aircraft chasing and ice cloud sampling were considered to perform a second PCA.

Then, the analysis is performed on the remaining angular scattering coefficients (4669 Angular Scattering Coefficients (ASC) representing PN measurements of flights 16b and 19b) now restricted to 25 angles θ ranging from 15° to 155°. The new set of variables or coordinates, C_{lj}, can be expressed with the scalar product of the vector of reduced angular scattering coefficients $\vec{\sigma_j}(\theta)$ for the j^{th} measurements, expressed in log scale, and the l^{th} eigenvector $\xi_l(\theta)$ (i.e. principal component) of the total data set correlation matrix (Jourdan et al., 2010).

$$C_{lj} = (\overrightarrow{\ln\sigma_j} - \langle\overrightarrow{\ln\sigma}\rangle)^T.\vec{\xi_l} \quad (4)$$

where $\langle\overrightarrow{\ln\sigma}\rangle$ represents the average ASC of the dataset.

The first three eigenvectors $\overrightarrow{\xi_l(\theta)}$ of the correlation matrix are displayed in Fig. 2 along with their normalized eigenvalues λ_l, representing more than 99% of the variability of the PN angular scattering coefficients (ASC).

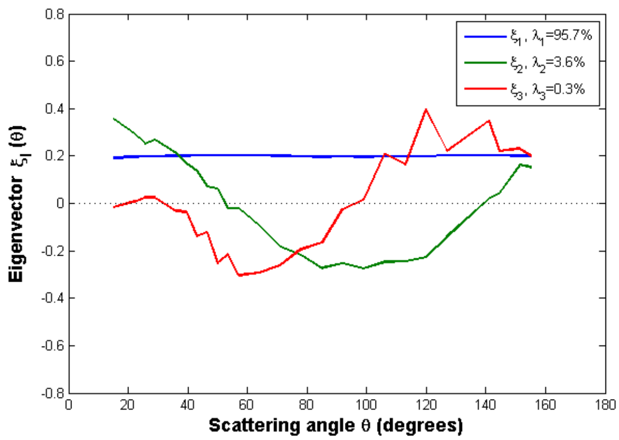

Figure 2 : First three eigenvectors for the flights 16b and 19b.

The first eigenvector $\xi_1(\theta)$ is approximately constant versus scattering angle and represents 95.7% of the total variance. It means that this principal component is representative of changes of the magnitude of phase functions without any changes in their global shape. This behavior means that 95.7% of the ASC variations are linked to changes of the cloud particle extinction. Results show a good correlation (r^2 = 0.98) between the first eigenvector and the extinction derived from the PN measurements (ExtPN).

The second eigenvector $\xi_2(\theta)$ reverses sign twice at scattering angles equal to 50° and 140° with an extremum around 90°. Accordingly, 3.6% of the angular scattering variability corresponds to a redistribution of scattered energy from the angular region (50°-140°) to scattering angles lower than 50° and higher than 140°. Light-scattering modeling studies demonstrate that the scattering behavior in the angular region between 60° and 140° is sensitive to the particle shape and thermodynamic phase (Jourdan et al., 2010). A strong linear correlation (r^2=0.97) between the second eigenvector and the asymmetry coefficient (gPN) at 804 nm is found.

The third eigenvector represents only 0.3% of the total variance. However, this eigenvector provides additional information in scattering regions which are not well described by the first two principal components. It has opposite signs in the angular region (30°-90°) and (90°-155°) with maximum extremal values at 60° and 120°. The shape of the third eigenvector describes the forward/backward hemisphere partitioning of the scattering. Baran et al. (2012), Xie et al. (2006), and Xie et al. (2009) showed that the scatter pattern for angles between 120° and 160°, corresponding to ice bow-like effects, is sensitive to quasi-spherical particles. Moreover, these backscattering angles (θ>120°) and scattering angles around 22° and 46° (corresponding to halo features) can also be linked to the particle habits and surface roughness (Xie et al., 2009, Jourdan et al., 2010).

Based on these three first principal components, each phase function (or ASC) measured by the PN

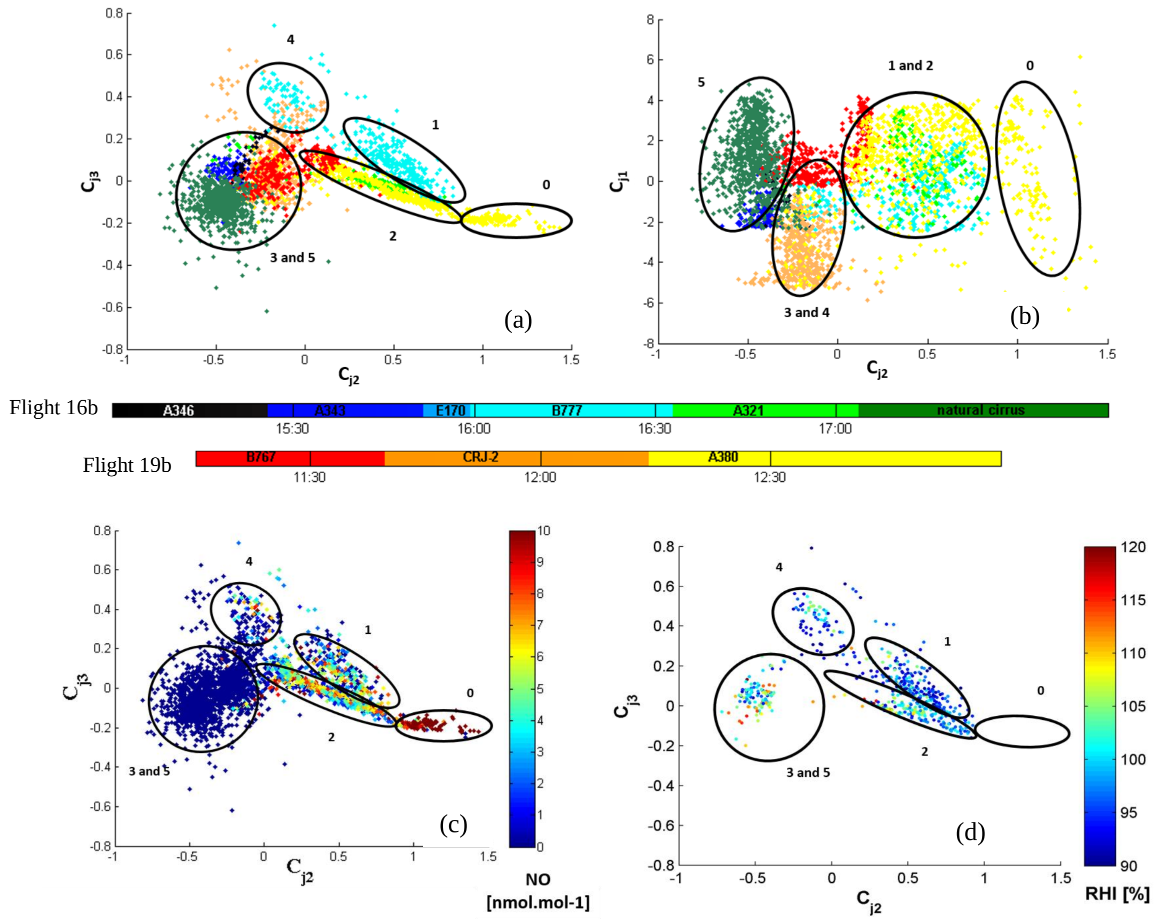

Figure 3: Expansion coefficient diagram for flights 16b and 19b (excluding 19b for RHI information): third versus second principal component for a), c) and d), and first versus second principal component for b). Data points are color coded according to ATC information for a) and b), by NO concentration for c), and by RHI values for d). The 6 typical scattering regimes (0-5) are indicated and numbered accordingly.

can be expressed with a good accuracy as a linear combination of these components (Jourdan et al., 2010). The PN data are projected into a new space defined by the three principal components (3D-space) instead of the 25-dimensional space of ASC. The scatterplots of the C_{j3} and C_{j1} expansion coefficients versus the C_{j2} coefficient are represented on Fig. 3a and b respectively. Fig. 3a illustrates the features of the ASC measurements in one of the most comprehensive way. Each point corresponds to a measured phase function documented over 25 angles. The variability of C_{j2} coefficients is significant with values ranging from -1 to 1.5. The angular variation of the second principal component indicates that large values of C_{j2} ($C_{j2} > 0.75$) correspond to ASC with low side scattering (60°-130°) and higher forward scattering (15°-40°) and somehow higher backscattering (145-155°). This behavior is connected to an increase of the asymmetry parameter with an increase of C_{j2} values. Thus, the fraction of spherical particles increases with increasing C_{j2}. In the region defined by negative values of C_{j2} the density of points is relatively high. These cloud events exhibit optical properties characterized by a large side scattering and low asymmetry parameter. Therefore, specific cloud sequences sharing similar scattering properties can be identified based on this second principal component. Young contrails characterized by quasi-spherical ice crystals have high positive values of C_{j2} while cirrus clouds and contrail cirrus exhibit high negative values.

In the space of the third principal component high positive values of C_{j3} imply that less energy is scattering in the forward hemisphere and thus more energy is scattered in the backward hemisphere. The variability of the expansion coefficients is less pronounced as ASC are distributed between -0.4 and 0.6. Most of the measured ASC do not significantly differ from the average ASC in the angular ranges (30°-90°) and (90°-155°). However, some specific clusters linked to scattering behavior can be identified for values of C_{j3} greater than 0.1 and lower than -0.1. These threshold values also depend of the position of the ASC on the second principal component. Finally, the first principal component is directly linked to the extinction coefficient. High values of C_{j1} are representative of optically dense cloud sequences.

Based on the time series displayed in Fig. 1, data points corresponding to contrails are also color coded according to their aircraft origin illustrated on Fig. 3a and b. From these information and based on the first three principal components, 6 clusters (see numbered ellipsoids in Fig. 3) representative of particular scattering behavior can be roughly identified. Figure 3a suggests an increase of C_{j2} and a decrease of C_{j1} with increasing aircraft size. Figure 3c shows an increase of C_{j2} for increasing NO mixing ratio. Some contrails or ice cloud events are clearly delimited by a single area in the C_{j3} versus C_{j2} and also C_{j2} versus C_{j1} diagrams. For instance cirrus clouds are gathered in cluster 5. Most of the contrails induced by the B767, A340 and CRJ2 aircraft are associated to cluster 3 or 5. It means that these cloud events share similar optical properties characterized by a low asymmetry parameter, high side scattering behavior, and supersaturated ambient conditions with respect to ice. More interestingly, Fig. 3 shows that some contrail events are smeared out over several areas or clusters. Contrails relative to the A380 aircraft are dispatched in cluster 0 and 2 while the ones corresponding to the B777 are spread out between clusters 1 and 4. This clearly indicates that the contrails are evolving in space and/or time along the Falcon flight track while chasing the respective contrails. This evolution can also be seen in the in-situ measurements of NO concentration color coded on Fig. 3c. Cloud regions influenced by air traffic can be discriminated from clouds formed by natural processes based on the NO concentration values. While clusters 3 and 5 are characterized by very low NO concentrations (close to zero) above background, clusters 0, 1, 2, and 4 correspond to higher concentrations representative of a significant aircraft exhaust influence. For instance, a clear trend shows that an increase of NO concentration translates into higher values of C_{j2}. Hence, contrails characterized by a low side scattering due to the presence of spherical ice crystals correspond to high NO concentration. This behavior can be a signature of young contrail properties. Elder or aged contrails composed of a higher fraction of non-spherical crystals or growing more aspherically are expected to exhibit an enhanced side scattering and a lower asymmetry parameter associated to lower NO concentrations.

The contrail and cirrus classification based on ASC measurements appears to be consistent with the independent trace gas measurements. Each cluster represented on Fig. 3 can be linked to a distinct cloud event. Therefore, the combination of flights 16b and 19b can provide a relevant test-bed database to discriminate contrail properties. Young contrails (spherical ice crystals) are associated to clusters 0, 1 or 2, whereas aged contrails (aspherical ice crystals and higher RHI values) with more pristine ice are categorized in clusters 3 and 4, and finally natural cirrus (low NO concentrations) are found in cluster 5. A less precise analysis (using onboard camera) reveals that cluster 0 corresponds essentially to the primary wake created below the secondary wake behind an aircraft. These different clusters are defined arbitrarily according to ATC information and according to their optical differences through the three first principal components. In the following, the clusters will be referenced according to the contrail evolution stage

- Cluster 0 : Primary Wake (PW)
- Cluster 1 : Young Contrail 1 (YC1)
- Cluster 2 : Young Contrail 2 (YC2)
- Cluster 3 : Aged Contrail Clean (ACC)
- Cluster 4 : Aged Contrail (AC)
- Cluster 5 : Cirrus Cloud (CC).

Thus, the next step is to validate these cluster definitions according to the different tracers. One has to keep in mind that some points are still arbitrarily attributed to a particular cluster without strong physical justification.

3.2.2 Application to other CONCERT flights

In this section we investigate the possibility to complement the previous analysis with additional cloud optical measurements performed during other CONCERT flights to increase the robustness of the method.

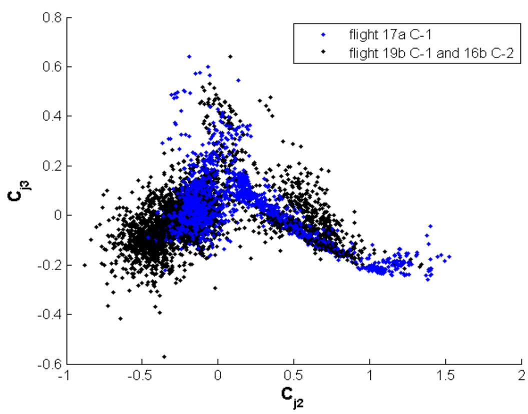

Figure 4: Example of data projection in the C_{j2}/C_{j3} space where data from flight 17a (blue data points) are superimposed on the data from the benchmark flights 19b and 16b (black data points).

The principal components obtained on the basis of the measurements performed during flight 16b and 19b are considered as our reference axes. Now, the ASC measured during other flights can be projected on this space of principal components. The coordinates of these flights are calculated from

Eq. (4). An example of this data projection is illustrated in Fig. 4 where flight 17a is represented in the C_{j2}/C_{j3} space. Every PCA data point can be attributed to one cluster previously defined by the PCA implemented with flights 16b and 19b data (black points). In other words, every ASC measured during another flight can be merged (projected) into the expansion coefficient diagram relative to the base measurements performed during flights 16b and 19b. Data points sharing similar optical properties will still be close to each other. According to the cluster definition, Fig. 4 shows that different contrail phases have been experienced during flight 17a. Data points are mostly grouped into cluster ACC, but are also present in clusters AC, YC2, and PW. Finally, cloud data encountered during this flight are mainly categorized as young and aged contrails.

We follow this methodology to project and classify each additional "contrail" flight performed during both CONCERT campaigns. In order to attribuate each measurement (or point) to one cluster and to enhance the statistical significance of our clustering analysis we compute the Mahalanobis distance (De Maesschalck et al., 2000). Clusters are defined by their means (or centers), standard deviations (or widths), and cross-correlations (or tilts). The Mahalanobis distance is given by the equation:

$$D_M(x)_i = \sqrt{(x - \mu_i)^T S_i^{-1} (x - \mu_i)} \tag{5}$$

with D_M the Mahalanobis distance between point χ and the i[th] cluster center, μ_i the N-dimensional mean of this cluster and S_i its covariance matrix. Each data point can be associated to a specific cluster corresponding to the shorter Mahalanobis distance, and the ellipsoids' eccentricity and width can be adjusted.

Day / Aitcraft		Cluster: PW (1st wake)	ACC (aged contrail)	AC (aged contrail)	YC1 (young contrail)	YC2 (young contrail)	CC (Cirrus)	Number of points	Age (s)
17a C-1	TOTAL							1435	
	A340-311							359	61 - 144
17b C-1	TOTAL							2715	
	B737-500							310	77 - 151
	A340-642							100	82 - 139
	NC							189	-
19a C-1	TOTAL							2152	
	A319-111							628	94 - 129
	A340-311							175	63 - 90
19b C-1	TOTAL							1647	
	B767-300							319	77 - 107
	CRJ-2							151	80 - 95
	A380-841							677	109 - 240
20 C-1	TOTAL							1434	
	B737-300							64	90 - 290
16b C-2	TOTAL							1511	
	A340-600							128	100 - 132
	B777							378	120 - 160
	A321							135	70 - 95
17 C-2	TOTAL							2904	
	NC1							498	-
	NC2							233	-
24 C-2	TOTAL							1380	
	B777							371	112 - 178

Table 1: Classification relative to the six clusters on the Cj2/Cj3 representation of the PCA of all data points for each flight of the two CONCERT campaigns (C-1 in November 2008 and C-2 in September 2011). The length of the bars represent the relative contribution of data points of individual contrails (blue bars) and also entire flights (black bars) to the 6 individual clusters.

The classification relative to the six clusters shown on the C_{j3} vs C_{j2} and the C_{j1} and C_{j2} expansion diagrams is summarized in Table 1. A total of 8 flights (6 additional flights) representing 4426 ASC measurements was processed. The lengths of the bars in Table 1 represent the relative contributions of data points to the different clusters: a) black bar merge cloud data points (with extinction coefficient higher than 0.1 km^{-1}) for entire flights and b) blue bars present individual aircraft contrails within specific flights. An important fraction (at least more than 30%) of data points is detected in clusters ACC and CC for each flight during the two campaigns. This indicates that these data points are sampled in aged contrail and sometimes natural cirrus. For flights more clearly performed in well visible contrails outside natural cirrus (earlier development stage and/or intensified persistent elder contrails), significant fractions of data points are associated to clusters PW, YC1, and YC2 (young contrails) for both CONCERT-1 and CONCERT-2 campaigns. However, these flights are also characterized by a significant contribution of data points to cluster ACC (aged contrails clean) and to a minor extent in cluster AC (aged contrails, mostly corresponding to measurements performed during two different B777 contrail chasing events).

These results are in reasonable agreement with previous conclusions (this subsection) about cluster definitions and associated contrail / ice cloud characteristics. Very young contrails have been chased during CONCERT-1 (flights 19a, 19b and 20) and during CONCERT-2 (flights 16b, 17 and 24). Another interesting result is related to flight 17 during CONCERT-2 (flight 17 C-2). No contrail information has been communicated from ATC, however the Falcon has been flying apparently in visible contrails, probably too old for ATC recognition. Data points can mainly be attributed to cluster CC, and to a minor extent to cluster ACC and cluster YC2. This observation suggests that significantly aged contrails have been sampled, resembling strikingly natural cirrus clouds. Indeed, crystal formation and growth processes in contrails and natural cirrus suggest that very old contrails more and more resemble natural cirrus properties. From Table 1 it is obvious that an important amount of data points had been sampled in natural cirrus during this flight. All these natural cirrus data points appear in the black bars but only to a minor extent in the blue bars limited to ATC communicated contrail sequences.

ATC information on contrail ages has been collected during each chasing. Some chasings have been performed less than 100 s after contrail formation. This is the case for the A340 contrail during flight 19a and for the CRJ-2 contrail during flight 19b of CONCERT-1 and for the A321 contrail during flight 16b of CONCERT-2. One can notice that the contrail ages are well correlated to chosen cluster definitions, revealing that contrail data relative to the A340 are included in cluster YC1 and YC2 (young contrails) for more than 53% of the data points, and nearly 65% for the CRJ-2 and 88% for the A321. According to our cluster classification, only 12% of the data points gathered during these three flights correspond to aged contrail (cluster ACC and AC) categories in contrast to other CONCERT-1 and CONCERT-2 flights (with more than 30% of data points associated to ACC and AC). Even though it is still difficult to associate contrail ages to measurement points, the “contrail age” ranges are in agreement with the cluster definitions.

4 Evolution of contrail properties

4.1 Optical and chemical cluster properties

As demonstrated in the previous part, cloud events can be separated according to their light-scattering properties. Six clusters were defined based on two flights with significant number of data points for each cluster. In this section we present mean optical, chemical, and microphysical properties for each of the six clusters. These mean properties have been calculated over all data points associated to the 6 individual clusters (all flights, both CONCERT campaigns). Figure 5a, 5c, and 5d illustrate the normalized frequency distributions of the asymmetry parameter (gPN), the extinction coefficient (ExtPN), and NO concentrations for the six clusters, respectively. Figure 5b represents mean normalized scattering phase functions, also for the 6 clusters.

Atmos. Chem. Phys. Discuss., https://doi.org/10.5194/acp-2017-946
Manuscript under review for journal Atmos. Chem. Phys.
Discussion started: 13 October 2017

Atmospheric Chemistry and Physics Discussions

The asymmetry parameter gPN statistics for the six clusters shown in Fig. 5a provide the most relevant information on cloud characteristics and the related context of contrail evolution/age. In agreement with findings in Gayet et al. (2012), aged contrails (cluster ACC and AC) and natural cirrus (cluster CC) correspond to gPN values between 0.72 and 0.80, younger contrails (cluster YC1 and YC2) to gPN between 0.80 and 0.86, and primary wake measurements (cluster PW) to gPN above 0.86. This result can be explained with the time evolution of ice crystal shapes after exhaust from quasi-spherical ice particle to, e.g. column, needle, bullet, and bullet-rosette type crystals. In the primary wake, the pressure increases associated in the descending vortex. This leads to adiabatic heating and subsequent sublimation processes of the ice crystals (Lewellen and Lewellen, 2001; Unterstrasser et al., 2016) and explains a return to spherical shapes and high values of the asymmetry coefficients.

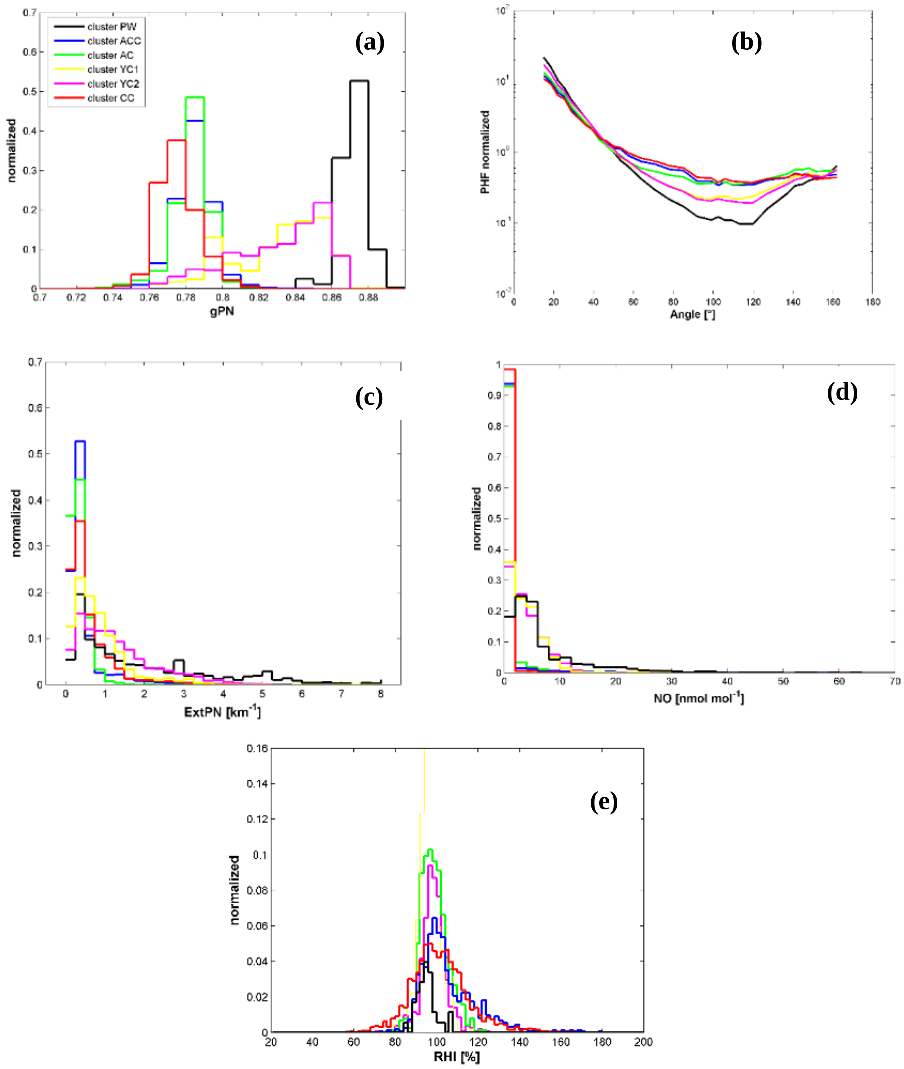

Figure 5: Normalized histograms of a) asymmetry coefficient, b) phase function, c) extinction retrieved by Polar Nephelomter, d) NO concentration for all flights, and e) RHI conditions for CONCERT-2 flights.

The normalized phase functions are presented in Fig. 5b. Primary wake phase functions (cluster PW) are clearly different from young contrail phase functions (cluster YC1 and YC2), which are themselves different from aged contrails (cluster ACC and AC) and natural cirrus (cluster CC) phase functions. The main difference between the averaged phase functions is observed for the side scattering region (50°-140°) which is related to changes of ice particles shapes and to the proportion of spherical ice crystals within the contrails. This behavior is expected and also in agreement with position of cluster PW, YC2 and YC1 on the expansion coefficient diagram (Fig. 2). The decrease of the C_{j2} coefficient is associated to a side scattering enhancement. Therefore, very young contrails composed of a majority of spherical ice crystals are characterized by phase functions with a substantial scattering at forward angles associated with much lower scattering at sideward angles. As the contrails evolve these features smooth out leading to phase functions with a featureless behavior and a more flat appearance at side scattering angles. Finally, the averaged normalized phase functions of old contrails and natural cirrus are resembling each other. This also explains that they are difficult to discriminate with the PCA.

The extinction coefficient statistics are presented in Fig. 5c. All the aged contrails (cluster ACC and AC) exhibit extinction coefficients lower than 2 km^{-1}. The same statement applies for 80% of the sampled natural cirrus (cluster CC). For younger contrails (cluster YC1 and YC2) extinction coefficients can reach 5 km^{-1}. Largest extinction coefficients are achieved in primary wake measurements sorted into cluster PW with extinction coefficients reaching values up to 8 km^{-1}. Still, the main fraction (more than 50% of data points) of young contrail data yields extinction coefficients between 0 and 1 km^{-1}.

Concentrations of chemical species also allow characterizing contrail/cirrus cloud data. The concentration depends strongly on the type of the pursued aircraft. Figure 5d shows mean concentrations of nitrogen oxide NO data points attributed to the six individual clusters. Young contrail NO concentrations (cluster PW, YC1 and YC2) can reach values up to 10 nmol mol^{-1} and up to 60 nmol mol^{-1} in the primary wake. In contrast, in aged contrails and in natural cirrus (cluster ACC, AC and CC) NO concentrations do not exceed 10 nmol mol^{-1} (which is true for more than 97.5%, 99.6%, and 99.7% of data points for clusters ACC, AC, and CC, respectively). Indeed, after exhaust, concentrations of nitrogen oxide NO and sulfur dioxide SO_2 created by combustion reactions decrease rapidly due to the dispersion in the upper troposphere and reactions with other molecules.

Finally, saturation conditions with respect to ice are presented in Fig. 5e for all clusters and for CONCERT-2 flights only. The predominant measured ambient relative humidity in all clusters is around 95%. Cluster ACC and CC (blue and red lines) show higher RHI values (more than 120%) than other clusters. Thus, this can explain the formation of natural cirrus and persistent contrails for these ambient conditions. Contrary to all other clusters, no supersaturation is observed for cluster PW (in black), defined as primary wake measurements. This result is in agreement with the definition of the primary wake, which is still in the non-persistent phase of the contrail.

The above results highlight that the principal component analysis, based on the ASC measurements described in Sect. 3, allows to discriminate different types of contrails. Specific optical and chemical properties can thus be characterized for each contrail phase and can be related to their evolution. An interesting aspect is that the PCA analysis facilitates to connect clusters of optical properties to microphysical characteristics of the contrails within specific clusters.

4.2 Microphysical cluster properties

Microphysical properties are assessed using the combination of FSSP-300 and 2DC measurements. They have been analyzed for each cluster for hydrometeor diameters between 0.5 µm and 800 µm.

Figure 6 shows mean volume particle size distributions (PSD) for all six clusters measured from the FSSP-300 and 2DC with respective limited instrumental size ranges. A linear interpolation in logarithmic space has been applied for each PSD in the size range from 17 µm to 70 µm which is not accurately documented by the two instruments. These results include all flights of the study (8 flights from CONCERT-1 and 2). It is important to note that more than 500 data points are included in each cluster with a maximum of 6300 data points for cluster ACC.

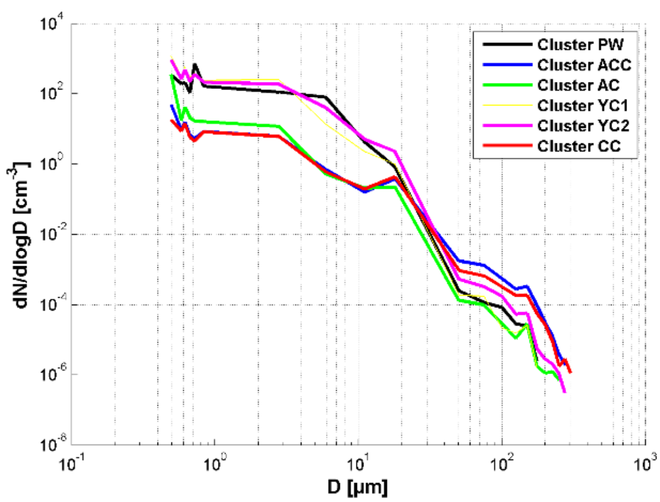

Figure 6: Number particle size distributions for each cluster including all data points of all flights. FSSP-300 measurements from 0.5 to 17 µm and 2DC measurements from 70 µm to 800 µm. The data are linearly interpolated in logarithm space between 17 µm and 70µm.

Figure 6 shows that the mean number PSDs for each cluster are consistent with the cluster definition. Indeed, two categories of PSD can be observed. Within the FSSP-300 size range, PSD relative to old contrails (cluster ACC and AC) and cirrus (cluster CC) exhibit more than one order of magnitude lower number concentrations of small ice crystal compared to young contrails (cluster YC1 and YC2) and primary wake (cluster PW). Within the two groups, no significant differences can be noticed due to uncertainties of the FSSP-300 number concentration measurements of 30% for concentrations around 5cm^{-3} and 75% for concentrations around 0.5 cm^{-3} (Gayet et al., 2002). The differences between these two groups can been explained by the production of small ice crystals in fresh exhaust plumes followed by rapid dilution during subsequent minutes after the exhaust. Within the 2DC range, the PSDs are also in agreement with the cluster definitions. A higher concentration of large ice crystals with diameters around 100 µm and beyond are expected for natural cirrus and significantly well-developed contrails. This is particularly well illustrated on the PSD in the 2D-C size range where a higher concentration of large ice crystal is observed for clusters ACC and CC compared to the younger contrails. However, these PSD do not allow discriminating young contrails in primary wake (cluster PW) from contrails in the secondary wake (cluster YC1 and YC2).

Extinction (km^{-1})		Mean	std	Mediane	prctile 25	prctile 75
cluster	PW	3,904	4,386	1,972	0,528	6,125
	ACC	0,088	0,282	0,028	0,009	0,057
	AC	0,079	0,186	0,024	0,001	0,071
	YC1	2,037	2,363	1,307	0,440	2,667
	YC2	2,163	2,816	1,227	0,316	2,634
	CC	0,113	0,237	0,065	0,030	0,127

IWC ($mg\ m^{-3}$)		Mean	std	Mediane	prctile 25	prctile 75
cluster	PW	15,46	21,56	6,26	0,87	22,79
	ACC	8,74	37,77	0,35	0,01	3,33
	AC	1,65	19,76	0,02	0,00	0,22
	YC1	5,29	11,45	1,46	0,17	5,78
	YC2	7,85	23,40	1,36	0,14	7,77
	CC	28,69	145,73	0,96	0,05	2,87

NTOTAL (cm^{-3})		Mean	std	Mediane	prctile 25	prctile 75
cluster	PW	125,94	98,37	109,54	54,24	166,57
	ACC	5,57	17,86	1,29	0,76	2,41
	AC	17,89	33,48	2,92	1,21	32,90
	YC1	155,80	159,42	106,65	38,43	207,70
	YC2	164,20	173,17	103,81	42,26	211,85
	CC	6,06	10,12	3,75	2,17	6,81

Table 2: Optical and microphysical properties for each cluster according interpolated particle size distributions from FSSP-300 and 2DC measurements.

Table 2 presents ice water content (IWC, in mg m^{-3}) and total number of ice crystals (NTOTAL, in particles cm^{-3}) derived from the measured PSD for each cluster. The extinction coefficient (in km^{-1}) obtained from the PN measurements is also displayed. Despite the large uncertainties associated to both instruments and the interpolation method (for ice crystals with diameters ranging from 17 µm and 70 µm), these results again prove that each cluster can be connected to specific contrail phases. The microphysical and optical properties of cluster PW are in agreement with the cloud properties excepted in the primary wakes. The extinction coefficient has a mean value of 3.9 km^{-1}, IWC is close to 15.5 mg m^{-3}, and the number concentration yields a typical value of 125 particles cm^{-3}. Young (clusters YC1 and YC2) and aged contrails (clusters ACC and AC) exhibit distinctive differences in their optical and microphysical properties. Higher extinction coefficients and ice number concentration, 2 km^{-1} and 160 cm^{-3}, respectively, characterize young contrails compared to aged contrails with 0.08 km^{-1} and 10 particles cm^{-3}, respectively. Cluster CC corresponds to natural cirrus clouds where significant atmospheric spreading and ice growth occurred. Thus, within this cluster the extinction coefficients (mean values of 0.1 km^{-1}) as well as the number concentration of ice crystals (around 6 particles cm^{-3}) are very low. The IWC is higher with a mean value of 28.7 mg m^{-3} due to ice crystal growth in supersaturated conditions.

However, it is difficult to discriminate young contrail cases (YC1 and YC2) based on their microphysical properties. Clusters ACC and AC microphysical properties are also similar but ACC IWC and number concentrations are closer to the ones of the cirrus case indicating a more evolved stage of the observed ACC contrail cluster.

Conclusions

In this study, a new form of statistical analysis of contrail to cirrus evolution is presented based on two intensive contrail measurement campaigns, CONCERT-1 and CONCERT-2. The data are used

Atmos. Chem. Phys. Discuss., https://doi.org/10.5194/acp-2017-946
Manuscript under review for journal Atmos. Chem. Phys.
Discussion started: 13 October 2017

to study optical and microphysical properties of contrails during their evolution from young contrails to contrail-cirrus clouds, and ambient natural cirrus clouds. The combination of optical, microphysical, and chemical airborne measurement data was used to present an extended view of cloud properties, and to merge those results with ATC flight information about sampled contrails.

A Principal Component Analysis (PCA) methodology has been applied to the measured Polar Nephelometer scattering phase function data in order to facilitate a distinction between cloud properties in different contrail phases. The PCA results were derived first for two reference flights that sampled contrails and cirrus in various development stages, including the primary wake, the young secondary wake, old contrails (few minutes after formation) and natural cirrus. For these flights, the PCA clearly demonstrates the potential to separate different groups of clouds, justifying the use of these two flights as a benchmark. The scattering phase functions measured during other CONCERT flights were then projected into the space of principal components obtained from the two reference flights. Mahalanobis distances were used to measure the separation between the additional data points and the data in the predefined clusters. From the entire data set, the cloud properties in the various contrail development stages can be separated and analyzed separately. The analysis demonstrates that the clearest separation between clusters is related to particle shape, which is significantly controlling the scattering phase function and the derived asymmetry parameter gPN. The asymmetry parameter clearly separates young contrails (gPN of 0.72 to 0.80) from contrail/cirrus with gPN ranging from 0.80 to 0.88. Since it is still difficult to evaluate the exact age of each measurement, young and aged contrails are classified also by their optical and chemical properties. The measured NO concentrations are useful to distinguish natural cirrus from old contrails. Despite the important gap between the two instruments used to measure particle size distributions, particle size spectra and related mean values of the ice particle number concentration, extinction and ice water content have been determined for each cluster. The various clusters clearly show different size distributions. In good agreement with previous findings on optical and chemical properties, we find that young contrails have more than a factor of ten higher number concentrations of small ice crystals (with diameters lower than 20 µm) than aged contrails and natural cirrus. On the other hand, aged contrails and natural cirrus contain larger ice crystals, with diameters larger than 75 µm. The optical and microphysical properties of the aged contrail cirrus are often similar to those found in the ambient "natural" cirrus clouds. The results show that the PCA method allows to identify and discriminate different contrail growth stages and to provide an independent method for the characterization of the evolution of contrail properties.

Accurate modeling of cirrus or contrails' single scattering properties is a primary condition for the interpretation of remote sensing measurements. Therefore, measurements of the optical characteristics of ice crystals in natural conditions are still needed for validation of numerical techniques and for the determination of free parameters in light scattering models. In this context, the results from the PCA could be used to develop representative parameterizations of the scattering and geometrical properties of the ice crystals' shapes and sizes observed in the visible wavelength range that then have to be extrapolated into the near infrared.

Acknowledgments

We thank financing by the Helmholtz Association under contract VH-NG-309 and W2/W3-60. Part of this work was funded by DFG SPP HALO 1294 contract VO1504/4-1, and by the DLR project Eco2Fly in ML-CIRRUS-cirrus special issue. We thank Lufthansa, the DLR flight department and DFS for excellent support during the campaign. The in-situ data can be found in the HALO-database (https://halo-db.pa.op.dlr.de/).

References

Baran, A.J., Gayet, J.-F., and Shcherbakov, V.: On the interpretation of an unusual in-situ measured ice crystal scattering phase function. *Atmospheric Chemistry and Physics* 12, 9355–9364, 2012.

Baumgardner, D., Dye, J.E., Gandrud, B.W., and Knollenberg, R.G.: Interpretation of measurements made by the forward scattering spectrometer probe (FSSP-300) during the Airborne Arctic Stratospheric Expedition. *Journal of Geophysical Research 97*, 8035–8046, 1992.

Borrmann, S., Luo, B., and Mishchenko, M.; Application of the T-Matrix Method to the Measurement of Aspherical (Ellipsoidal) Particles with Forward Scattering Optical Particle Counters. *Journal of Aerosol Science* 31, no. 7 (2000): 789–799, 2000.

Burkhardt, U., Kärcher, B., and Schumann, U.: Global modeling of the contrail and contrail cirrus climate impact. *Bulletin of the American Meteorological Society* 91, 479–484, 2010.

Burkhardt, U. and Kärcher, B.: Global radiative forcing from contrail cirrus. *Nature Climate Change*, 1(1), 54–58, 2011.

Carleton, A.M., Silva, A.D., Aghazarian, M.S., Bernhardt, J., Travis, D.J., and Allard, J.: Mid-season climate diagnostics of jet contrail “outbreaks” and implications for eastern US sky-cover trends. *Climate Research*, 56, 209–230, 2013.

Chen, C.-C. and Gettelman, A.: Simulated 2050 aviation radiative forcing from contrails and aerosols. *Atmospheric Chemistry and Physics*, 16(11), 7317–7333, 2016.

Duda, D. P., Minnis, P., Khlopenkov, K., Chee, T.L., and Boeke, R.: Estimation of 2006 Northern Hemisphere Contrail Coverage Using MODIS Data. *Geophysical Research Letters*, 40, 612-617, doi:10.1002/grl.50097, 2013.

Febvre, G., Gayet, J.-F., Minikin, A., Schlager, H., Shcherbakov, V., Jourdan, O., Busen, R., Fiebig, M., Kärcher, B., and Schumann, U.: On optical and microphysical characteristics of contrails and cirrus. *Journal of Geophysical Research: Atmospheres* (1984–2012) 114, 2009.

Frömming, C., Ponater, M., Dahlmann, K., Grewe, V., Lee, D.S., and Sausen, R.: Aviation-induced radiative forcing and surface temperature change in dependency of the emission altitude. *Journal of Geophysical Research: Atmospheres* (1984–2012) 117, 2012.

Gayet, J.-F., Auriol, F., Minikin, A., Ström, J., Seifert, M., Krejci, R., Petzold, A., Febvre, G., and Schumann, U.: Quantitative Measurement of the Microphysical and Optical Properties of Cirrus Clouds with Four Different in Situ Probes: Evidence of Small Ice Crystals. *Geophysical Research Letters* 29, no. 24: 2230. doi:10.1029/2001GL014342, 2002.

Gayet, J.F., Crépel, O., Fournol, J.F., and Oshchepkov, S.: A new airborne Polar Nephelometer for the measurements of optical and microphysical cloud properties. Part I: Theoretical design. *In Annales Geophysicae*, pp. 451–459, 1997.

Gayet, J.-F., Ovarlez J., Shcherbakov, V., Ström, J., Schumann, U., Minikin, A., Auriol, F., Petzold, A., and Monier M.: Cirrus Cloud Microphysical and Optical Properties at Southern and Northern Midlatitudes during the INCA Experiment. *Journal of Geophysical Research: Atmospheres* 109, no. D20 : D20206. doi:10.1029/2004JD004803, 2004.

Gayet, J.-F., Shcherbakov, V., Voigt, C., Schumann, U., Schäuble, D., Jeßberger, P., Petzold, A., Minikin, A., Schlager, H., Dubovik, O., and Lapyonok, T.: The evolution of microphysical and optical properties of an A380 contrail in the vortex phase. *Atmospheric Chemistry and Physics*. *12*, 6629–6643, 2012.

Garrett, T.J., Gerber, H., Baumgardner, D.G., Twohy, C.H., and Weinstock, E.M.: Small, highly reflective ice crystals in low-latitude cirrus. *Geophysical Research Letters* 30, 2132, 2003.

Gettelman, A., and Chen, C.: The climate impact of aviation aerosols. *Geophysical Research Letters*, 40, 2785–2789, doi:10.1002/grl.50520, 2013.

Gierens, K. and Dilger, F.: A climatology of formation conditions for aerodynamic contrails, *Atmospheric Chemistry and Physics*, 13, 10847-10857, doi:10.5194/acp-13-10847-2013, 2013.

Graf, K., Schumann, U., Mannstein, H., and Mayer, B.: Aviation induced diurnal North Atlantic cirrus cover cycle. *Geophysical Research Letters* 39, L16804, doi:10.1029/2012GL052590, 2012.

Goodman, J., Pueschel, R.F., Jensen, E.J., Verma, S., Ferry, G.V., Howard, S.D., Kinne, S.A., and Baumgardner, D.: Shape and size of contrails ice particles. *Geophysical Research Letters* 25, 1327–1330, 1998.

Heller, R., Voigt, C., Beaton, S., Dörnbrack, A., Kaufmann, S., Schlager, H., Wagner, J., Young, K., and Rapp, M.: Mountain waves modulate the water vapor distribution in the UTLS, *Atmospheric Chemistry and Physics, Discussion*, doi:10.5194/acp-2017-334, in review.

Heymsfield, A., Baumgardner, D., DeMott, P., Forster, P., Gierens, K., and Kärcher, B.: Contrail Microphysics. *Bulletin of the American Meteorological Society* 91, 465–472, 2010.

Heymsfield, A.J., and Parrish, J.L.: A computational technique for increasing the effective sampling volume of the PMS two-dimensional particle size spectrometer. *Journal of Applied Meteorology* 17, 1566–1572, 1978.

Irvine, E.A., Hoskins, B.J., and Shine, K.P.: The dependence of contrail formation on the weather pattern and altitude in the North Atlantic. *Geophysical Research Letters* 39, L12802, doi:10.1029/2012GL051909, 2012.

Järvinen, E., Schnaiter, M., Mioche, G., Jourdan, O., Shcherbakov, V.N., Costa, A., Afchine, A., Krämer, M., Heidelberg, F., Jurkat, T., Voigt, C., Schlager, H., Nichman, L., Gallagher, M., Hirst, E., Schmitt, C., Bansemer, A., Heymsfield, A., Lawson, P., Tricoli, U., Pfeilsticker, K., Vochezer, P., Möhler, O., and Leisner, T.: Quasi-spherical Ice in Convective Clouds, *Journal of Atmospheric Sciences*, doi:10.1175/JAS-D-15-0365.1, 2016.

Jansen, J. and Heymsfield, A. J.: Microphysics of aerodynamic contrail formation processes, *Journal of Atmospheric Sciences*, 72(9), 3293–3308, 2015.

Jeßberger, P., Voigt, C., Schumann, U., Sölch, I., Schlager, H., Kaufmann, S., Petzold, A., Schäuble, D., and Gayet, J.F.: Aircraft type influence on contrail properties, *Atmospheric Chemistry and Physics*, 13, 11965-11984, doi:10.5194/acp-13-11965-2013, 2013.

Jourdan, O., Mioche, G., Garrett, T.J., Schwarzenböck, A., Vidot, J., Xie, Y., Shcherbakov, V., Yang, P., and Gayet, J.-F.: Coupling of the microphysical and optical properties of an Arctic nimbostratus cloud during the ASTAR 2004 experiment: Implications for light-scattering modeling. *Journal of Geophysical Research: Atmospheres* (1984–2012) 115, 2010.

Jourdan, O., Oshchepkov, S., Gayet, J.-F., Shcherbakov, V., and Isaka, H.: Statistical analysis of cloud light scattering and microphysical properties obtained from airborne measurements. *Journal of Geophysical Research* 108, 4155, 2003.

Jurkat, T., Kaufmann, S., Voigt, C., Schäuble, D., Jeßberger, P., and Ziereis, H.: The airborne mass spectrometer AIMS – Part 2: Measurements of trace gases with stratospheric or tropospheric origin in the UTLS, *Atmospheric Measurement Technics*, 9, 1907–1923, doi:10.5194/amt-9-1907-2016, 2016.

Jurkat, T., Voigt, C., Arnold, F., Schlager, H., Aufmhoff, H., Schmale, J., Schneider, J., Lichtenstern, M., and Dörnbrack, A.: Airborne stratospheric ITCIMS-measurements of SO_2, HCl, and HNO_3 in the aged plume of volcano Kasatochi, *Journal of Geophysical Research*, 115, D00L17, doi:10.1029/2010JD013890, 2010.

Jurkat, T., Voigt, C., Arnold, F., Schlager, H., Kleffmann, J., Aufmhoff, H., Schäuble, D., Schäfer, M., and Schumann, U.: Measurements of HONO, NO, NOy and SO2 in aircraft exhaust plumes at cruise, *Geophysical Research Letters*, 38, L10807, doi:10.1029/2011GL046884, 2011.

Kärcher, B., and Voigt, C.: Formation of nitric acid/water ice particles in cirrus clouds, *Geophysical Research Letters*, 33, L08806, doi:10.1029/ 2006GL025927, 2006.

Kärcher, B., and Voigt, C.: Susceptibility of contrail ice crystal numbers to aircraft soot particle emissions, *Geophysical Research Letters*, 44, 8037-8046, doi:10.1002/2017GL074949, 2017.

Kärcher, B., and Yu, F.: Role of aircraft soot emissions in contrail formation. *Geophysical Research Letters*, 36, L01804, doi:10.1029/2008GL036649, 2009.

Kaufmann, S., Voigt, C., Jeßberger, P., Jurkat, T., Schlager, H., Schwarzenboeck, A., Klingebiel, M., and Thornberry, T.: In situ measurements of ice saturation in young contrails, *Geophysical Research Letters*, 41, doi:10.1002/2013GL058276, 2014.

Kaufmann, S., Voigt, C., Jurkat, T., Thornberry, T., Fahey, D. W., Gao, R.-S., Schlage, R., Schäuble, D., and Zöger, M.: The airborne mass spectrometer AIMS – Part 1: AIMS-H_2O for UTLS water vapor measurements, *Atmospheric Measurement Technics*, 9, 939-953, doi:10.5194/amt-9-939-2016, 2016.

Kübbeler, M., Hildebrandt, M., Meyer, J., Schiller, C., Hamburger, Th., Jurkat, T., Minikin, A., Petzold, A., Rautenhaus, M., Schlager, H., Schumann, U., Voigt, C., Spichtinger, P., Gayet, J.-F., Gourbeyre, C., and Krämer, M.: Thin and subvisible cirrus and contrails in a subsaturated environment, *Atmospheric Chemistry and Physics*, 11, 5853-5865, doi:10.5194/acp-11-5853-2011, 2011.

Lawson, R.P., O'Connor, D., Zmarzly, P., Weaver, K., Baker, B., Mo, Q., and Jonsson, H.: The 2D-S (stereo) probe: Design and preliminary tests of a new airborne, high-speed, high-resolution particle imaging probe. *Journal of Atmospheric and Oceanic Technology* 23, 1462–1477, 2006.

Lee, D.S., Pitari, G., Grewe, V., Gierens, K., Penner, J.E., Petzold, A., Prather, M.J., Schumann, U., Bais, A., and Berntsen, T.: Transport impacts on atmosphere and climate: Aviation. *Atmospheric Environment* 44, 4678–4734, 2010.

Legendre, P., and Legendre, L.: Numerical Ecology, 2nd English ed., 853 pp., *Elsevier Science*, New York, 1998.

De León, R.R., Krämer, M., Lee, D.S., and Thelen, J.C.: Sensitivity of radiative properties of persistent contrails to the ice water path. *Atmospheric Chemistry and Physics*. 12, 7893–7901, 2012.

Lewellen, D.C.: Analytic solutions for evolving size distributions of spherical crystals or droplets undergoing diffusional growth in different regimes. *Journal of the Atmospheric Sciences* 69, 417–434, 2012.

Lewellen, D.C., and Lewellen, W.S.: The effects of aircraft wake dynamics on contrail development. *Journal of the Atmospheric Sciences* 58, 390–406, 2001.

Liou, K.N., Takano, Y., Yue, Q., and Yang, P.: On the radiative forcing of contrail cirrus contaminated by black carbon. *Geophysical Research Letters*, 40, 778–784, doi:10.1002/grl.50110, 2013.

De Maesschalck, R., Jouan-Rimbaud, D., and Massart, D.L.: The Mahalanobis Distance. *Chemometrics and Intelligent Laboratory Systems* 50, no. 1: 1–18. doi:10.1016/S0169-7439(99)00047-7, 2010.

Meyer, J., Rolf, C., Schiller, C., Rohs, S., Spelten, N., Afchine, A., Zöger, M., Sitnikov, N., Thornberry, T. D., Rollins, A. W., Bozóki, Z., Tátrai, D., Ebert, V., Kühnreich, B., Mackrodt, P., Möhler, O., Saathoff, H., Rosenlof, K. H., and Krämer, M.: Two decades of water vapor measurements with the FISH fluorescence hygrometer: a review, *Atmospheric Chemistry and Physics*, 15, 8521–8538, doi:10.5194/acp-15-8521-2015, 2015.

Mishchenko, M.I., Travis, L.D., Kahn, R.A., and West, R.A.: Modeling phase functions for dustlike tropospheric aerosols using a shape mixture of randomly oriented polydisperse spheroids. *Journal of Geophysical Research 102*, 16831–16, 1997.

Moore, R. H., Thornhill, K. L., Weinzierl, B., Sauer, D., D'Ascoli, E., Kim, J., Lichtenstern, M., Scheibe, M., Beaton, B., Beyersdorf, A. J., Barrick, J., Bulzan, D., Corr, C. A., Crosbie, E., Jurkat, T., Martin, R., Riddick, D., Shook, M., Slover, G., Voigt, C., White, R., Winstead, E., Yasky, R., Ziemba, L. D., Brown, A., Schlager, H., and Anderson, B. E.: Biofuel blending reduces particle emissions from aircraft engines at cruise conditions, *Nature*, 543, 411-415, 10.1038/nature21420, 2017.

Schäuble, D., Voigt, C., Kärcher, B., Stock, P., Schlager, H., Krämer, M., Schiller, C., Bauer, R., Spelten, N., De Reus, M.., Szakáll, M., Borrmann, S., Weers, U., and Peter T.: Airborne measurements of the nitric acid partitioning in persistent contrails, *Atmospheric Chemistry and Physics*, 9, 8189-8197, 2009.

Atmos. Chem. Phys. Discuss., https://doi.org/10.5194/acp-2017-946
Manuscript under review for journal Atmos. Chem. Phys.
Discussion started: 13 October 2017

Atmospheric Chemistry and Physics
Open Access
Discussions

Schlager, H., Konopka, P., Schulte, P., Schumann, U., Ziereis, H., Arnold, F., Klemm, M., Hagen, D.E., Whitefield, P.D., and Ovarlez, J.: In situ observations of air traffic emission signatures in the North Atlantic flight corridor. *Journal of Geophysical Research 102*, 10739–10, 1997.

Schröder, F., Kärcher, B., Duroure, C., Ström, J., Petzold, A., Gayet, J.-F., Strauss, B., Wendling, P., and Borrmann, S.: On the Transition of Contrails into Cirrus Clouds. *Journal of the Atmospheric Sciences* 57, 464–480, 2000.

Schumann, U.: On conditions for contrail formation from aircraft exhausts. *Meteorologische Zeitschrift*, *5*, 4–23, 1996.

Schumann, U., Baumann, R., Baumgardner, D., Bedka, S. T., Duda, D. P., Freudenthaler, V., Gayet, J.-F., Heymsfield, A. J., Minnis, P., Quante, M., Raschke, E., Schlager, H., Vázquez-Navarro, M., Voigt, C. and Wang, Z.: Properties of individual contrails: a compilation of observations and some comparisons, *Atmospheric Chemistry and Physics*, 17(1), 403–438, doi:10.5194/acp-17-403-2017, 2017b.

Schumann, U., and Heymsfield, A.: On the lifecycle of individual contrails and contrail cirrus, *Meteorological Monographs*, 58, 3.1-3.24, doi: 10.1175/AMSMONOGRAPHS-D-16-0005.1, 2017.

Schumann, U., Jeßberger, P., and Voigt, C.: Contrail ice particles in aircraft wakes and their climatic importance, *Geophysical Research Letters*, 40, 2867-2872, doi: 10.1002/grl.50539, 2013.

Schumann, U., Kiemle, C., Schlager, H., Weigel, R., Borrmann, S., D'Amato, F., Krämer, M., Matthey, R., Protat, A., Voigt, C., and Volk, C. M.: Long-lived contrails and convective cirrus above the tropical tropopause, *Atmospheric Chemistry and Physics*, 17, 2311-2346, doi:10.5194/acp-17-2311-2017, 2017a.

Schumann, U., Mayer, B., Gierens, K., Unterstrasser, S., Jessberger, P., Petzold, A., Voigt, C., and Gayet, J.-F.: Effective Radius of Ice Particles in Cirrus and Contrails. *Journal of the Atmospheric Sciences*, 68, 300–321, 2011.

Schumann, U., Penner, J.E., Chen, Y., Zhou, C., and Graf, K.: Dehydration effects from contrails in a coupled contrail-climate model, *Atmospheric Chemistry and Physics*, 15, 11179-11199, doi: 10.5194/acp-15-11179-2015, 2015.

Shcherbakov, V., Jourdan, O., Voigt, C., Gayet, J.F., Chauvigne, A., Schwarzenboeck, A., Minikin, A., Klingebiel, M., Weigel, R., Borrmann, S., Jurkat, T., Kaufmann, S., Schlage, R., Gourbeyre, C., Febvre, G., Lapyonok, T., Frey, W., Molleker, S., and Weinzierl, B.: Porous Aerosol in Degassing Plumes of Mt. Etna and Mt. Stromboli. *Atmospheric Chemistry Physics* 16, no. 18: 11883–97. doi:10.5194/acp-16-11883-2016, 2016.

Sussmann, R., and Gierens, K.M.: Lidar and numerical studies on the different evolution of vortex pair and secondary wake in young contrails. *Journal of Geophysical Research: Atmospheres* 104, 2131–2142, 1999.

Sussmann, R., and Gierens, K.M.: Differences in early contrail evolution of two-engine versus four-engine aircraft: Lidar measurements and numerical simulations. *Journal of Geophysical Research: Atmospheres* 106, 4899–4911, 2001.

Vazquez-Navarro, M., Mannstein, H. and Kox, S.: Contrail life cycle and properties from 1 year of MSG/SEVIRI rapid-scan images, *Atmospheric Chemistry and Physics*, 15(15), 8739–8749, 2015.

Voigt, C., Jessberger, P., Jurkat, T., Kaufmann, S., Baumann, R., Schlager, H., Bobrowski, N., Giuffrida, G., and Salerno, G.: Evolution of CO2, SO2, HCl, and HNO3 in the Volcanic Plumes from Etna. *Geophysical Research Letters*, 41, 6, 2196-2203. doi:10.1002/2013GL058974, 2014.

Voigt C., Schlager, H., Ziereis, H., Kärcher, B., Luo, B.P., Schiller, C., Krämer, M., Popp, P.J., Irie, H., and Kondo, Y.: Nitric acid in cirrus clouds, *Geophysical Research Letters*, 33, L05803, doi:10.1029/2005GL025159, 2006.

Voigt, C., Schumann, U., Jurkat, T., Schäuble, D., Schlager, H., Petzold, A., Gayet, J.-F., Krämer, M., Schneider, J., Borrmann, S., Schmale, J., Jessberger, P., Hamburger, T., Lichtenstern, M., Scheibe, M., Gourbeyre, C., Meyer, J., Kübbeler, M., Frey, W., Kalesse, H., Butler, T., Lawrence, M.G., Holzäpfel. F., Arnold, F., Wendisch, M., Döpelheuer, A., Gottschaldt, K., Baumann, R., Zöger, M., Sölch, I., Rautenhaus, M., and Dörnbrack, A.: In-situ observations of young contrails - Overview and selected case studies from the CONCERT campaign, *Atmospheric Chemistry and Physics*, 10, 9039–9056, doi:10.5194/acp-10-9039-2010, 2010.

Voigt, C., Schumann, U., Jessberger, P., Jurkat, T., Petzold, A., Gayet, J.-F., Krämer, M., Thornberry, T., and Fahey, D.: Extinction and optical depth of contrails, *Geophysical Research Letters*, 38, L11806, doi:10.1029/2011GL04718, 2011.

Voigt, C., Schumann, U., Minikin, A., Abdelmonem, A., Afchine, A., Borrmann, S., Boettcher, M., Buchholz, B., Bugliaro, L., Costa, A., Curtius, J., Dollner, M., Dörnbrack, A., Dreiling, V., Ebert, V., Ehrlich, A., Fix, A., Forster, L., Frank, F., Fütterer, D., Giez, A., Graf, K., Grooß, J.-U., Groß, S., Heimerl, K., Heinold, B., Hüneke, T., Järvinen, E., Jurkat, T., Kaufmann, S., Kenntner, M., Klingebiel, M., Klimach, T., Kohl, R., Krämer, M., Krisna, T. C., Luebke, A., Mayer, B., Mertes, S., Molleker, S., Petzold, A., Pfeilsticker, K., Port, M., Rapp, M., Reutter, P., Rolf, C., Rose, D., Sauer, D., Schäfler, A., Schlage, R., Schnaiter, M., Schneider, J., Spelten, N., Spichtinger, P., Stock, P., Walser, A., Weigel, R., Weinzierl, B., Wendisch, M., Werner, F., Wernli, H., Wirth, M., Zahn, A., Ziereis, H., and Zöger, M.: ML-CIRRUS - The airborne experiment on natural cirrus and contrail cirrus with the high-altitude long-range research aircraft HALO, *Bulletin of the American Meteorological Society*, doi: 10.1175/BAMS-D-15-00213, 2017.

Xie, Y., Yang, P., Gao, B.-C., Kattawar, G.W., and Mishchenko, M.I.: Effect of ice crystal shape and effective size on snow bidirectional reflectance. *Journal of Quantitative Spectroscopy and Radiative Transfer* 100, 457–469, 2006.

Xie, Y., Yang, P., Kattawar, G.W., Minnis, P., and Hu, Y.X.: Effect of the inhomogeneity of ice crystals on retrieving ice cloud optical thickness and effective particle size. *Journal of Geophysical Research: Atmospheres* (1984–2012) 114, 2009.

Yang, P., Hong, G., Dessler, A.E., Ou, S.S., Liou, K.-N., and Minnis, P.: Contrails and induced cirrus: Optics and radiation. *Bulletin of the American Meteorological Society* 91, 473–478, 2010.

Ziereis, H., Schlager, H., Schulte, P., Velthoven, P. van, and Slemr, F.: Distributions of NO, NO x, and NO y in the upper troposphere and lower stratosphere between 28 and 61 N during POLINAT 2. *Journal of Geophysical Research: Atmospheres* (1984–2012) 105, 3653–3664, 2000.

Zöger, M., Afchine, A., Eicke, N., Gerhards, M-T., Klein, E., McKenna, D.S., Mörschel, U., Schmidt, U., Tan, V., Tuitjer, F., Woyke, T., Schiller, C. : Fast in situ stratospheric hygrometers: A new family of balloon-borne and airborne Lyman alpha photofragment fluorescence hygrometers. *Journal of Geophysical Research: Atmospheres*, 104, 1807-1816, 1999.